Fisheries Research 260 (2023) 106585

Contents lists available at ScienceDirect

Fisheries Research

journal homepage: www.elsevier.com/locate/fishres

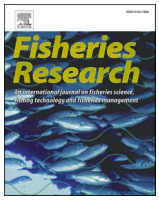

Remote acoustic sizing of tethered fish using broadband acoustics

Rokas Kubilius [a,*], Benoît Bergès [b], Gavin J. Macaulay [a]

[a] Institute of Marine Research, P.O. Box 1870 Nordnes, NO-5817 Bergen, Norway
[b] Wageningen Marine Research, Haringkade 1, 1976 CP IJmuiden, Netherlands

ARTICLE INFO

Keywords:
Acoustic
Broadband
Echosounder
Fish
Size

ABSTRACT

Remote fish sizing is desirable in fisheries (e.g., pre-catch) and research (e.g., platforms without biological sampling capacity) applications. In those contexts, the high spatial resolution of pulse compressed broadband echoes combined with narrow beamwidth transducers makes it feasible to resolve the scattering from different parts of the fish body and hence can be used to measure the body size. A motorized apparatus was used to suspend individual fish in the acoustic beam of two laterally oriented transducers (45–90 kHz, 160–260 kHz, 12.2 m range) with precise control of rotation angle. Broadband scattering was measured from tethered Atlantic mackerel (*Scomber scombrus*), saithe (*Pollachius virens*), and pollack (*Pollachius pollachius*) ranging in standard length from 239 to 491 mm as a function of orientation angle to validate sizing based on the acoustic resolution of fish body parts. Under these controlled conditions, fish size was underestimated by 11–19 mm, varying with broadband pulse characteristics, orientation angle, species, and fish size. The best remote acoustic sizing results were obtained using 160–260 kHz pulses with a slow rise and fall of pulse amplitude (aka, taper).

1. Introduction

Fish size is an essential descriptive parameter in fish biology, fisheries research, stock assessment and management, and fish harvesting via size-dependent market pricing. Size is often measured visually with manual methods, for example, by the use of measurement boards (Wollaston, 1928; Davenport and Hakling, 1965; Øvredal and Totland, 2002). Semi-manual and automated optics-based methods are also frequently used to size fishes in a variety of environments, such as a conveyor belt, fish holding net pens, in-situ, and fish within the cod-end of an actively fishing trawl (Strachan, 1994; Shortis et al., 2009; Rosen and Holst, 2013; Muñoz-Benavent et al., 2018). However, fish size information obtained via visual or direct sampling methods is practical only at short ranges from the observing equipment, catching vessel or associated gear. These are unsuitable in situations where fish would preferably be sized at range (for example, greater than 10 m), where biological sampling is not possible or practicable, and to provide size information before deploying the fishing gear. Active acoustics, on the other hand, is a tool with sufficient operational range, sensitivity, and sampling rate to be practical for timely sensing of fish size during both pelagic fishing operations and sampling by scientific gear such as acoustic-equipped platforms (e.g., drones, probes, moorings, and drifters).

Pre-capture species and size composition are vital pieces of information for oceanic fishing operations, such as pelagic trawling and purse seining. These harvesting methods can suffer from a lack of target selectivity that leads to suboptimal utilisation of quotas, discards, and slipping of fish that may result in significant unwanted fish mortality (Huse and Vold, 2010; Poos et al., 2010; Tenningen et al., 2012). Fish species can be judged remotely with reasonable accuracy using prior experience (location, time of year) and tools such as sonars (via school morphology, behaviour, acoustic frequency response). Pre-catch information about fish size, however, is not readily available in a convenient and practical manner and to an accuracy suitable for fishing operations.

Fish size estimation without biological sampling is of relevance for stock assessment and research purposes, especially so when using acoustic surveying platforms that cannot obtain physical samples of the surveyed species. This includes drifters or fish aggregating devices, moorings, autonomous underwater vehicles, and surface drones that are increasingly being used to supplement stock assessment efforts (De Robertis et al., 2019).

Sizing fish with active acoustics has used swimbladder resonance, acoustic frequency response, and average target strength to fish length relationships (Hawkins, 1977; McClatchie et al., 1996; Johnsen et al., 2009; Stanton et al., 2010). Swimbladder resonance is not a convenient method to size individual fishes as it requires the identification of the

* Corresponding author.
E-mail address: rokas.kubilius@hi.no (R. Kubilius).

https://doi.org/10.1016/j.fishres.2022.106585
Received 19 September 2022; Received in revised form 6 December 2022; Accepted 7 December 2022
Available online 19 December 2022
0165-7836/© 2022 The Author(s). Published by Elsevier B.V. This is an open access article under the CC BY license (http://creativecommons.org/licenses/by/4.0/).

resonance frequency which typically occurs at low frequencies relative to those used in common active acoustic surveying systems. In addition, resonance is ineffective on fish without a gas-filled swimbladder. Frequency response sizing methods are susceptible to fish behaviour and thus are not well suited to measuring size of individual fishes. Acoustic target strength is a stochastic measure that is ineffective when applied to individual fish because of large fish to fish and temporal variability (Simmonds and MacLennan, 2005). In contrast, the apparent size of an individual fish body dimension along the acoustic axis can be measured directly from the acoustic signal if sufficiently high range resolution is available. Matched filtering (also termed pulse compression) applied to frequency modulated pulses (chirps) provides a range resolution that is inversely proportional to the pulse bandwidth (Ehrenberg and Torkelson, 2000; Stanton et al., 2003), is independent of the pulse duration, and can achieve a sufficiently high spatial range resolution to resolve parts of a fish (Kubilius et al., 2020), while retaining an operational range that is useful in pelagic fishing operations. The limits and accuracy of such a direct acoustic sizing method has been studied using prolate spheroids made of a material with similar acoustic backscatter properties to that of fish flesh; they could size objects longer than 200 mm and wider than 20 mm (Kubilius et al., 2020). The broadband scattering from a fish, however, is more complex due to an abundance of internal structures with disparate impedance contrasts (Forland et al., 2014). Therefore, while boundary transitions found in artificial fish-like objects can be used to size that object with relative ease (Kubilius et al., 2020) the applicability to fish needs to be investigated.

In this paper we demonstrate that i) by using pulse-compressed broadband signals the major internal sound scattering structures of fish can be distinguished from the total scattering of the fish, ii) the body length of both gas-filled swimbladder-bearing and bladderless fishes can be measured remotely and directly. We also present a processing algorithm to autonomously extract fish size from broadband acoustic data. The potential for, and limitations of, direct acoustic fish sizing in the open sea are also discussed.

2. Material and methods

Tethered individuals of saithe (*Pollachius virens*) and pollack (*Pollachius pollachius*), two physoclisti species with closed gas-filled swimbladders, and Atlantic mackerel (*Scomber scombrus*), a species without a swimbladder, were ensonified with broadband acoustic pulses in seawater (September 2018 for mackerel and June 2019 for saithe and pollack). The location, methods and apparatus used to do this have been described (Kubilius et al., 2020), with the main difference for the current

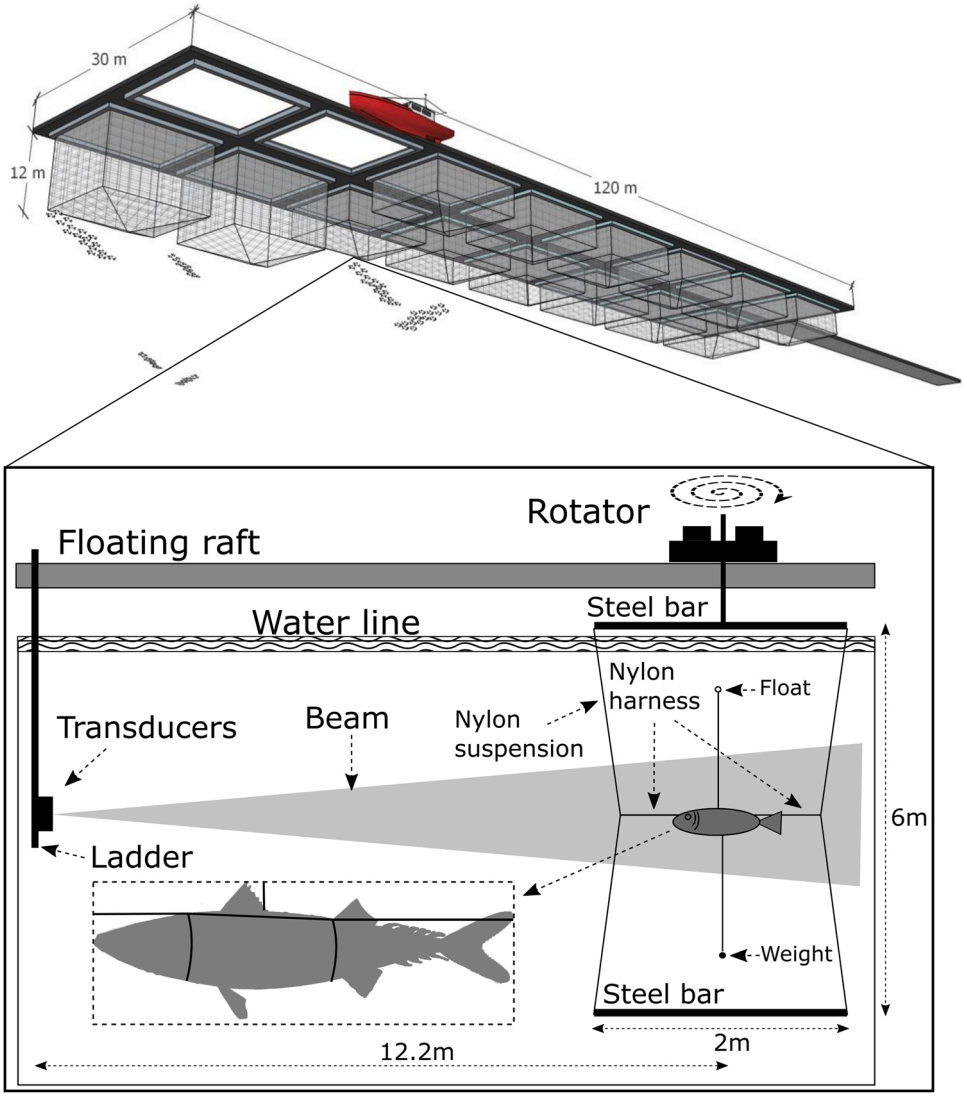

Fig. 1. Fish measurement apparatus and net-pen configuration. Floating net-pen platform (top) from which rotator, fish suspension setup, and echosounders were deployed (bottom). A small float (mackerel) or weight (saithe, pollack) was used to keep fish body upright. Modified after Kubilius et al. (2020).

work that the target suspension arrangement was adapted to accommodate fish instead of artificial targets (Fig. 1). Specifically, a small weight (saithe, pollack) or a float (mackerel) was attached to the fish by a monofilament line (arranged so that float or weight was vertically separated by 2 m from the target and hence outside the acoustic beam) to counteract the positive or negative buoyancy, and to keep an upright body posture as it was suspended in the water column.

2.1. Fish handling

Wild fish were caught at the experiment location, sedated, and terminated prior to the acoustic measurements. The treatment and use of fish in these experiments were approved by the Norwegian Food Safety Authority (FOTS 13717, 18/50881).

Mackerel, saithe, and pollack are attracted to and aggregate around the net-pen facilities at some periods of the year – all of the mackerel and pollack, and about half the saithe used were obtained from this source immediately prior to starting the acoustic backscatter measurements on each fish. The remainder of the saithe were obtained from the same wild population but were held in a net pen (12×12×12 m) from three weeks prior to the acoustic measurements. These fish were fed daily with fish feed pellets.

Each fish was caught by pole-and-line at 5–7 m depth, sedated in Finquel MS-222 (tricaine methanesulfonate) compound solution (100–200 mg l^{-1}), then terminated in a second solution of higher concentration (500–700 mg l^{-1}). The fish were not exposed to air between catching and suspension in the measurement apparatus. The time between capture and start of each acoustic measurement was 20–40 min. Acoustic backscatter data were recorded for 24 mackerel, 27 saithe, and 5 pollack (Table 1). Data from some of the fish were not used due to the onset of rigor mortis during the measurements, which significantly altered fish body posture. At times, wave action due to wind caused large relative motion between the transducer and fish and resulted in poor quality data – data from these fish were also removed from further analysis. After completion of the acoustic measurements, all saithe and pollack were frozen at − 20 °C within 2 h of fish capture for later x-ray imaging. Some mackerel were also frozen for x-ray imaging, although these were different fish to those used for the acoustic measurements.

2.2. X-ray imaging

The frozen fish were radiographed laterally and dorso-ventrally using a portable x-ray source (Hiray Plus) and detector plate (Canon CXDI-410 C) at 88 cm distance with source settings of 40 kV and 10 mA three months after being frozen. The x-ray data were saved into DICOM-formatted files with a 0.125 × 0.125 mm spatial resolution and x-ray absorption measures that varied from 0 (low absorption) to 65535 (high absorption). These were analysed to obtain swimbladder dimensions using the ImageJ software (Fig. 2). The maximum swimbladder length and maximum width (SBL and SBW respectively, Table 1) were defined as the longest dimension along (side aspect image, Fig. 2 C, E) and transverse (dorsal aspect image, Fig. 2 D, F) of the swimbladder respectively. A metal reference object of known length (a 41.1 mm long scalpel blade) was placed to the side of each fish as a reference length.

2.3. X-ray image and acoustic-derived fish length comparison

The accuracy of the acoustic backscatter-based fish size estimation was evaluated by comparison to sizes derived from the x-ray images. The dorsal-aspect fish x-ray images were processed to provide pseudo acoustic backscatter data as a function of rotation angle by treating the x-ray absorption data as a proxy for fish acoustic impedance (under the assumption that higher x-ray absorption occurs in denser material which has a higher impedance). The background of the backscatter images was cleaned and set to a value of 0 and the centre of the fish estimated as halfway along a line between the head and tail of the fish. The position of the pseudo acoustic source was defined to be at a range matching the actual fish experiments (specific to each individual fish) and all x-ray values within radius bands of 1 mm summed to yield a pseudo backscatter for that range band. The angle from the fish axis to the 'source' was changed in 1° steps and the range summations repeated to yield a matrix of pseudo backscatter as a function of range and rotation angle which is similar in characteristic to that observed from the acoustic datasets of rotated fish. The position of the fish boundaries was then calculated as a function of the rotation angle.

The pseudo acoustic backscatter data obtained from x-ray images was used to estimate the size of the fish by resolving the extent of fish body parts using simple thresholding. The accuracy of the acoustic data-derived fish size estimation was then evaluated using the following ratio:

$$r_{\mathrm{est}}(\theta_i:\theta_j) = \frac{s_{\mathrm{ac}}(\theta_i:\theta_j)}{s_{\mathrm{xray}}(\theta_i:\theta_j)}, \quad (1)$$

where $s_{\mathrm{ac}}(\theta_i:\theta_j)$ is the fish size in the rotation angle bin θ_i to θ_j infered

Table 1
Fish characteristics; total length (L-1), standard length (L-2), maximum width (W) and weight (Wt). Saithe and pollack swimbladder length (SBL) and maximum width (SBW) were measured from x-ray images. First character of the fish ID gives the species ("M" for mackerel, "S" for saithe, and "P" stand for pollack).

Fish ID	L-1 [mm]	L-2 [mm]	W [mm]	SBL [mm]	SBW [mm]	Wt [g]
M07	300	273	37	–	–	190
M10	356	323	46	–	–	386
M11	273	247	34	–	–	142
M12	375	342	48	–	–	408
M14	281	251	32	–	–	116
M15	465	421	66	–	–	982
M17	436	394	60	–	–	766
M18	378	343	47	–	–	406
M19	291	266	34	–	–	164
M20	319	290	45	–	–	278
M21	364	331	47	–	–	402
M22	455	413	64	–	–	988
M23	284	259	34	–	–	158
S01	470	433	60	191.4	21.6	1174
S02	434	393	64	182.4	24.5	926
S03	454	415	70	188.6	22.3	1135
S04	475	434	67	197.9	26.7	1318
S05	454	412	62	186.6	28.1	1124
S06	465	422	60	195.2	26.5	1118
S07	435	402	50	180.0	31.6	664
S08	413	381	54	169.2	23.1	760
S09	465	426	68	192.2	25.6	1222
S10	451	422	55	185.7	23.3	980
S11	422	390	58	173.0	21.1	822
S12	494	461	64	208.7	24.9	1386
S13	520	491	67	228.6	28.0	1624
S14	473	435	57	202.6	24.6	1094
S15	497	458	59	210.4	26.8	1186
S16	522	481	71	218.5	32.2	1664
S17	453	420	54	185.4	24.3	886
S18	401	373	47	164.6	20.3	700
S19	407	373	45	155.1	32.7	552
S20	402	370	50	163.6	23.7	698
S21	507	470	58	208.9	30.3	1234
S22	397	367	51	162.6	26.9	688
S23	299	279	31	115.7	20.0	258
S24	525	487	68	220.4	33.6	1618
S25	280	258	35	111.6	15.8	224
S26	505	472	69	209.9	35.6	1378
S27	372	340	48	133.9	29.4	536
P01	330	297	35	89.9	18.3	282
P02	266	241	27	102.5	14.7	154
P03	392	360	39	150.1	20.1	514
P04	371	342	38	146.2	20.1	446
P05	262	239	25	97.5	14.7	134

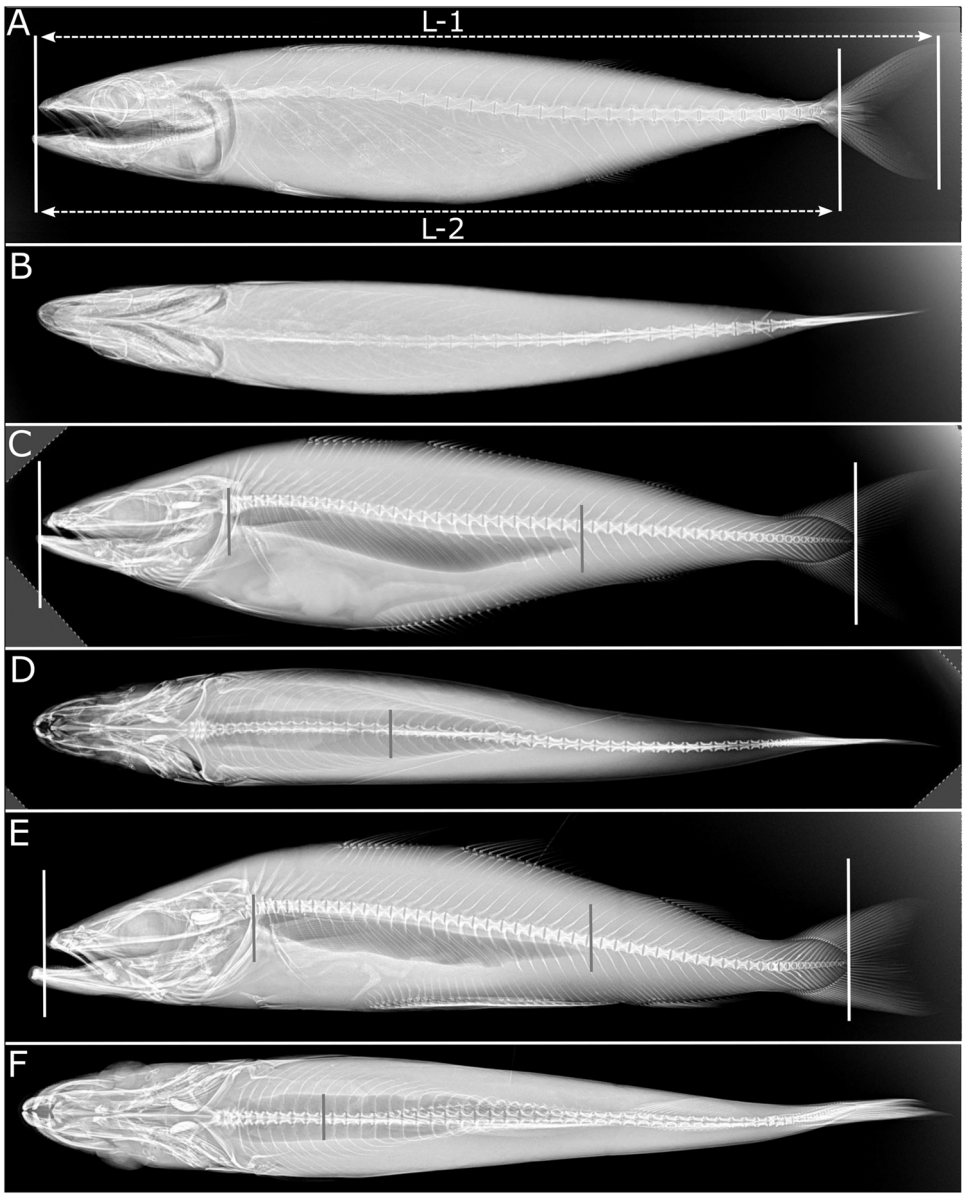

Fig. 2. Lateral and dorsal aspect x-rays of mackerel (A-B), saithe (C-D), and pollack (E-F). Fish total length (L-1), standard length (L-2), swimbladder length (distance between the two grey vertical lines in C and E), and maximum width (length of the vertical grey line in D and F) are indicated.

from the acoustic backscatter data, and $s_{\mathrm{xray}}(\theta_i : \theta_j)$ is the fish size in the rotation angle bin θ_i to θ_j inferred from the x-ray image. A value of $r_{\mathrm{est}}(\theta_i : \theta_j) = 1$ exemplifies a perfect match between the acoustic data and x-ray image derived fish size estimates in the corresponding rotation angle bin.

2.4. Fish suspension and rotation

The lateral acoustic incidence angle upon the fish was varied by rotating the fish about its' dorsal axis (Fig. 1). The fish were held by two loops formed as part of a horizontally stretched monofilament nylon line (the diameter of which varied with fish size, from 0.10 to 0.15 mm). One loop was positioned behind the pectoral fins and the second was placed in front of the second (mackerel) or third (saithe and pollack) dorsal fin. To keep the fish vertically oriented it was necessary to attach a weight or a float to the body, but which was located out of the acoustic beam. The mackerel were negatively buoyant and were held upright with the help of a small piece of cork and a 4 m long, 0.10 mm diameter monofilament nylon line (Fig. 1). This was passed through the back end of the first pectoral fin close to the skin and both free ends affixed to the cork, which was then 2 m above the fish. The saithe and pollack were positively buoyant and were held upright using a small lead weight (selected to suit the fish size), instead of the cork. The attachment line was passed through the front part of the first anal fin. All of these manipulations took place with the fish underwater. The rest of the fish suspension apparatus (Fig. 1) consisted of vertical nylon suspension lines, two horizontal steel bars (one 50 mm above the surface and the second 6 m below the surface) and a rotation apparatus as per Kubilius et al. (2020).

The rotation apparatus (and hence the suspended fish) revolved at 2.1° s^{-1} and the rotation angle was saved at 10 Hz with a precision of 0.1°. Rotation angles of 0° and 180° corresponded to broadside ensonification. A rotation angle of 90° corresponded to head-on ensonification for mackerel, and tail-on for saithe and pollack (Fig. 3).

2.5. Echosounder and acoustic measurements

Backscatter from the fish was measured with a broadband split-aperture echosounder (Simrad EK80 transceivers and two transducers)

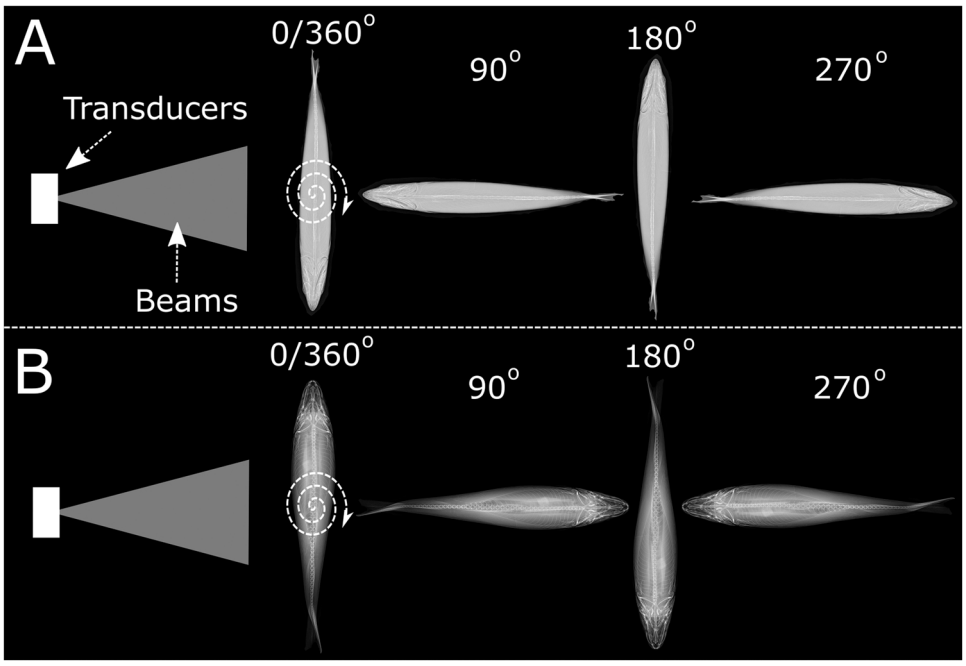

Fig. 3. Fish body rotation as viewed from above. Fish body postures at varying azimuth rotation angle during the acoustic backscatter recordings of mackerel (A) and saithe and pollack (B). All fishes were rotated clockwise.

producing simultaneous 45–90 and 160–260 kHz frequency-modulated upsweep pulses with the choice of slow and fast pulse amplitude tapering (Fig. 1, Table 2). The echosounder was calibrated using standard methods (Demer et al., 2015) and spherical target (38.1 mm diameter tungsten carbide sphere with 6% cobalt binder). The two transducers were mounted side-by-side at 3 m depth oriented to project towards the fish at about 12.2 m range (Fig. 1). The fish was suspended so it was positioned at the mid-point between the two acoustic beam centres (Kubilius et al., 2020). The acoustic backscatter data were stored from a minimum of 4 rotations of the fish with fast and slow tapered pulses – all the other settings were unchanged, generating four replicates for each measured fish. Daily measurements of seawater salinity and temperature at 3 m depth were entered into the echosounder software from which sound speed (Fofonoff and Millard Jr, 1983) and acoustic absorption (Francois and Garrison, 1982) was derived.

Table 2
Echosounder and acoustic configurations for mackerel (2018 September), saithe and pollack (2019 June) measurements. f_0 is the nominal frequency for the pulse bandwidth (70 and 200 kHz). Sound speed estimate (at 3 m depth) was obtained daily. Absorption coefficient is from the first day of measurements within each set.

Parameter	2018 September		2019 June	
Transducer type	ES70–7CD	ES200–7CD	ES70–7CD	ES200–7CD
Bandwidth [kHz]	45–90	160–260	45–90	160–260
Transmit power [W]	150	60	50	60
Fast power taper [%]	4.3	1.2	4.3	1.2
Slow power taper [%]	50	50	50	50
Gain at f_0 [dB]	27.0	26.7	27.7	26.5
Equivalent beam angle at f_0 [dB]	-20.7	-20.7	-20.7	-20.7
Absorption coefficient at f_0 [dB km^{-1}]	20.8	58.6	22.5	52.3
Half-power beam widths (alongship/ athwartship) at f_0 [°]	6.9/6.8	6.7/6.6	6.7/6.8	6.4/6.7
Pulse duration [ms]	1.024	1.024	1.024	1.024
Ping interval [s]	0.33	0.33	0.33	0.33
Sound speed [m s^{-1}]	1500.7–1502.2		1487.0–1496.3	

2.6. Acoustic data processing

The echosounder provided data files containing measurements of the backscattered acoustic energy for each ping as the fish were rotated (Fig. 4). The overall acoustic data processing workflow consisted of the following steps: i) identify backscatter from fish target, ii) detect the backscatter amplitude peaks that occurred at the boundary transitions within the fish body, iii) statistical analysis to yield estimates of apparent fish size along the acoustic axis as a function of incidence angle.

2.6.1. Backscatter processing

Several pre-processing steps were undertaken prior to size estimation. Firstly, the raw broadband acoustic signals were pulse compressed and the volume backscattering coefficients (S_v, dB re 1 m^{-1} (MacLennan et al., 2002)) were calculated by means of the sonar equation (MacLennan et al., 2002; Simmonds and MacLennan, 2005), i.e. accounting for sound absorption, spreading losses, and calibration gain. Secondly, echoes from the suspension lines that appeared in front of or behind the fish along the acoustic axis were suppressed using a mask. This mask was built by: i) detecting the suspension line echo traces at different rotation angles using the data from the 160–260 kHz channel, ii) fitting a polynomial of degree two as a function of rotation angle to determine the range-from-transducer window boundaries in which the fish echo traces are located. Echoes from the vertical suspension lines and the fish overlapped at the broadside observation aspect and when this occurred the range-from-transducer window boundaries were defined as ± 0.2 m to the range point that correspond to the centre of fish rotation. The mask was applied to both the 45–90 and 160–260 kHz data channels. Finally, species-specific lower S_v thresholds were applied (Table 3).

The acoustic backscattering strength from the fish body sound scattering boundaries varied with the rotation angle. For the sound scattering boundary detection algorithm to work optimally, it was important to retain the echo signal from the fish boundaries while rejecting background noise as effectively as possible. For the 160–260 kHz channel, a fixed S_v threshold level above the background noise level could be defined across the entire 360° of fish body angles. However, for

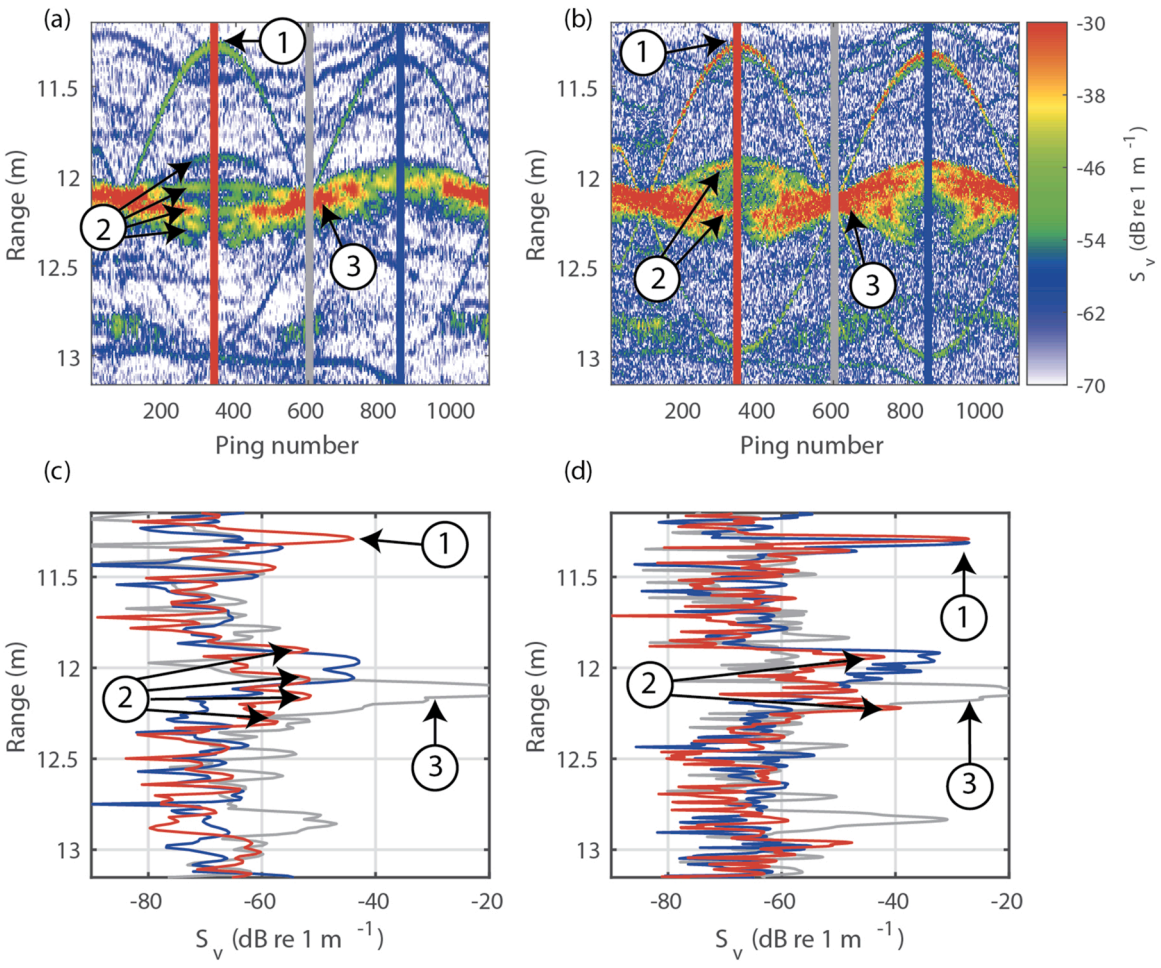

Fig. 4. Example echograms for saithe (S24) at (a) 45–90 kHz and (b) 160–260 kHz (slow taper) over single full rotation cycle (0°–360°). (c) and (d) show amplitude of three individual pings in (a) and (b), respectively. The red vertical stripes (a, b) and corresponding solid lines (c, d) are for fish observed at a tail-on aspect. The grey lines – fish observed at a broadside aspect. The blue stripes and lines indicate fish observed at a head-on aspect. Indicated on the graph are: (1) the echo traces of the vertical suspension lines; (2) the fish at tail-on aspect exemplifying multiple peaks corresponding to the candidate within-fish boundaries; (3) fish at broadside aspect exemplifying a single wide peak.

Table 3
Acoustic data processing parameters.

	Mackerel				Saithe, Pollack			
Frequency [kHz]	45–90		160–260		45–90		160–260	
Pulse taper	Fast	Slow	Fast	Slow	Fast	Slow	Fast	Slow
Upper threshold level [dB]	-34	-34	-34	-34	-34	-34	-34	-34
Lower threshold level [dB]	-60–55*	-60–55*	-50	-50	-60–55*	-60–55*	-50	-50
Prominence level [dB]	1–2*	2.5–5*	1–2*	1–2*	1–2*	1–2*	1–2*	1–2*
Moving average [#]	10	5	10	5	10	5	10	5
SNR** threshold [dB]	12	12	11	11	12	12	10	10
Rotation angle bin size (°)	20	20	5	5	20	20	5	5

* - adaptive choice of threshold or prominence level within the given value range.
** - signal-to-noise ratio; for definition see text Section 2.6.2.

the 45–90 kHz channel, the backscattering originating from the fish body parts was close to the background noise level at oblique angles whilst it was well above background noise at broadside angles. To minimize false positive detections at oblique angles, while maximizing true positives at broadside angles, the S_v threshold was defined as a function of rotation angle for the 45–90 kHz channel.

2.6.2. *Detection of fish body boundary transitions*

A 0.8 m wide range window centred at the mid-point of fish rotation (e.g., 12.15 m in Fig. 4) was selected for signal peak detection. Prior to the peak detection, the S_v time series was smoothed using a moving average (Fig. 5). The span of the moving average was chosen to minimize signal variability between peaks and optimize the peak detection process. A span of 5 samples at 45–90 kHz and 10 samples at 160–260 kHz were found to be optimal to suppress noise. These corresponded to 59.7 mm and 39.8 mm range, respectively. This discrepancy in the span of the moving average is due to the difference in range resolution and scattering characteristics at 45–90 kHz and 160–260 kHz. A peak detection algorithm was then applied based on: (1) a minimum distance between peaks of 20 mm, (2) case-specific

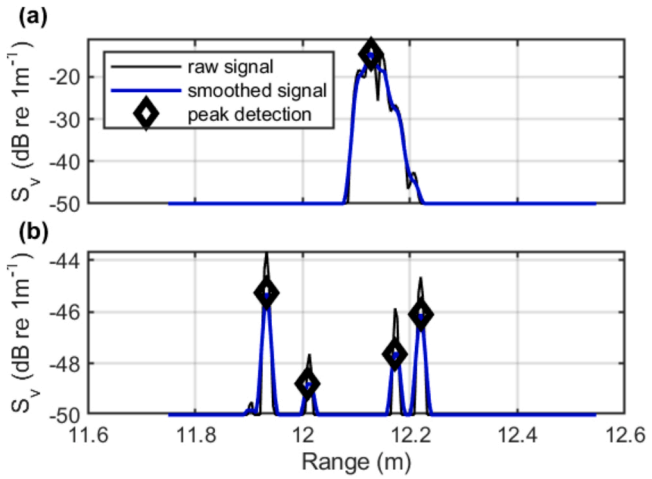

Fig. 5. Example of signal processing of S_v time series (160–260 kHz, slow taper, saithe S24). Prior to the peak detection (diamond markers), the raw S_v (black solid line) is smoothed using a moving average (blue solid line). (a) peak detection for a ping at 180° rotation angle (fish body at broadside). (b) processing for a ping at 90° rotation angle (tail-on aspect).

adaptive peak prominence levels (Table 3). The prominence level was defined as the S_v range between the potential peak and the surrounding minima. The detected amplitude peaks were only retained if their location in the acoustic beam was within 2° of the beam centre, as estimated by the split-aperture feature of the echosounder.

The signal-to-noise ratio (SNR) for each ping was computed within the 0.8 m signal peak detection window as:

$$SNR = \frac{\sqrt{\frac{1}{N_{sig}}\sum_{i=1}^{N_{sig}} s_{v_i}^{sig}}}{\sqrt{\frac{1}{N_{noise}}\sum_{i=1}^{N_{noise}} s_{v_i}^{noise}}} \quad (2)$$

The samples of the time series corresponding to effective signal $S_{v_i}^{sig}$ (with $S_{v_i}^{sig} = 10\log_{10}\left(s_{v_i}^{sig}\right)$) were taken as the samples within the 3 dB drop before and after each detected signal peak. The remainder of the samples in the 0.8 m window were taken to be the background noise $S_{v_i}^{sig}$ (with $S_{v_i}^{sig} = 10\log_{10}\left(s_{v_i}^{sig}\right)$). The SNR was used to identify and discard pings for which the peak detection was adversely affected by noise (Table 3).

2.6.3. *Statistical processing of peak detections*

For each measured fish, the range of the peak detections (Fig. 6a) were grouped into rotation angle bins (20° at 45–90 kHz and 5° at 160–260 kHz, Fig. 6b). A larger bin size was chosen for 45–90 kHz because the lower range resolution produced a smaller number of detections and a larger bin size was required to achieve statistical significance in the number of samples in each bin size. For each rotation angle bin, the probability density function (pdf) was estimated using a Gaussian kernel density function with 128 mesh points. The pdfs were further normalised relative to the maximum in each pdf (Fig. 6c) to construct the acoustic profile for each fish. The high points in the pdf (Fig. 6c) are range-to-peak values that correspond to the numerous detections within that rotation angle bin. These are associated with the acoustically reflective body parts of each fish specimen.

The acoustic profile was then converted into a binary image using a 0.5 threshold on the normalised pdf level (Fig. 6d). A morphological closing of the binary image was then applied using a disk element of 10-pixel radius. The resulting mask encompasses the range region where the extent of the fish was detected (Fig. 6e). Finally, size estimations in each rotation angle bins were inferred from the distance between the maximum and minimum ranges of the mask (Fig. 6f). The estimated total fish length was defined as the maximum size across all rotation angle bins. This point was generally reached at oblique target angles, either close head-on or tail-on orientations (90° or 270° rotation angle, Fig. 3).

3. Results

The acoustic backscatter was analysed for 13 mackerel, 27 saithe and 5 pollack (Table 1). The average of the daily estimates of seawater sound speed at the fish depth was 1501.4 (± 0.9) m s^{-1} for 2018 and 1490.7 (± 2.6) m s^{-1} for 2019 (Table 2).

The echo traces from the suspended fish and the suspension lines were clearly defined at both 45–90 kHz and 160–260 kHz (Fig. 4). Echoes from these were well separated except for an overlap when at a similar range from the transducer, i.e. at rotation angles of about 0° and 180° (pings 50 and 600 in Figs. 4a and 4b). The echoes from various parts of the fish body, such as the swimbladder, were also visible with varyable clarity.

The pulse-compressed signal peaks occurring at fish body boundary transitions were detected at different ranges from the transducers (Figs. 4, 5). The per-ping count and location of peak detections varied with rotation angle, target size, and fish species (Figs. 4, 6a). The inter-peak distances along the range axis varied with rotation angle. At tail-on or head-on rotation angles, one was able to discriminate fish body parts, while at broadside the echo peaks tended to merge (Figs. 4, 5).

The acoustically derived apparent fish body length was generally shorter than the manually measured one (Fig. 7). The 160–260 kHz pulses produced more accurate fish size estimates than the 45–90 kHz pulses and slow tapered signals performed better than fast (Fig. 8). The fish body length was estimated at head-on or tail-on fish body posture (Fig. 4) with considerable variability, notably for mackerel 45–90 kHz data (Fig. 9). Size measures were least variable for slow taper 160–260 kHz pulses (Fig. 9d) where 84% (27 out of 32) of pollack and saithe were measured within ± 25° of head-on or tail-on rotation angles (the ± 25° angular range was selected to encompass observations that correspond to fish swimming towards or away from the transducer). Mackerel size measures were more variable with only 7 of 13 fishes falling within that ± 25° range. Mackerel was about equally likely to be estimated for size as observed head on or tail on along the acoustic axis (54% and 46%, respectively for pooled data in Fig. 9). Finally, saithe was measured at tail on body posture 74% of the time (pooled data in Fig. 9) with this number being 78% for 160–260 kHz slow taper pulses.

The acoustically measured fish length correlated well with both the standard (L-2) and the total fish lengths (L-1) (Table 4) while being closer to the standard fish length (Fig. 7). The mackerel, saithe, and pollack standard body length (L-2) was underestimated on average by 13 mm (5%), 19 mm (7%), and 11 mm (3%), respectively, when sized with 160–260 kHz slow-tapered pulses. These numbers were 115 mm, 99 mm, and 101 mm, respectively, when sized with 45–90 kHz slow-tapered pulses. In all combinations of the bandwidth and taper type, the fitted linear regression yielded significant trends (p-values, Table 4). The residuals around the regression lines were generally equally distributed with no evidence of size-dependent trends in sizing ability (Fig. 7).

Fish size estimates derived from the pseudo acoustic, x-ray image-based data (Fig. 10) correlated well with direct acoustic sizing results by 160-260 kHz slow taper pulses (Fig. 11), subject to SNR, species, and fish length. The acoustic echo-based fish size estimates were on average 0.8% higher than those infered from the pseudo acoustic fish size measures for saithe and pollack at a SNR of 15–21 dB for size grouping between 20 and 50 cm (pooled data for saithe and pollack in Fig. 11). In this comparison there was a slight tendency for fish size- and SNR-dependent trends for saithe and pollack (Fig. 11), within the SNR and fish body size limits that were measured. The comparative measures of

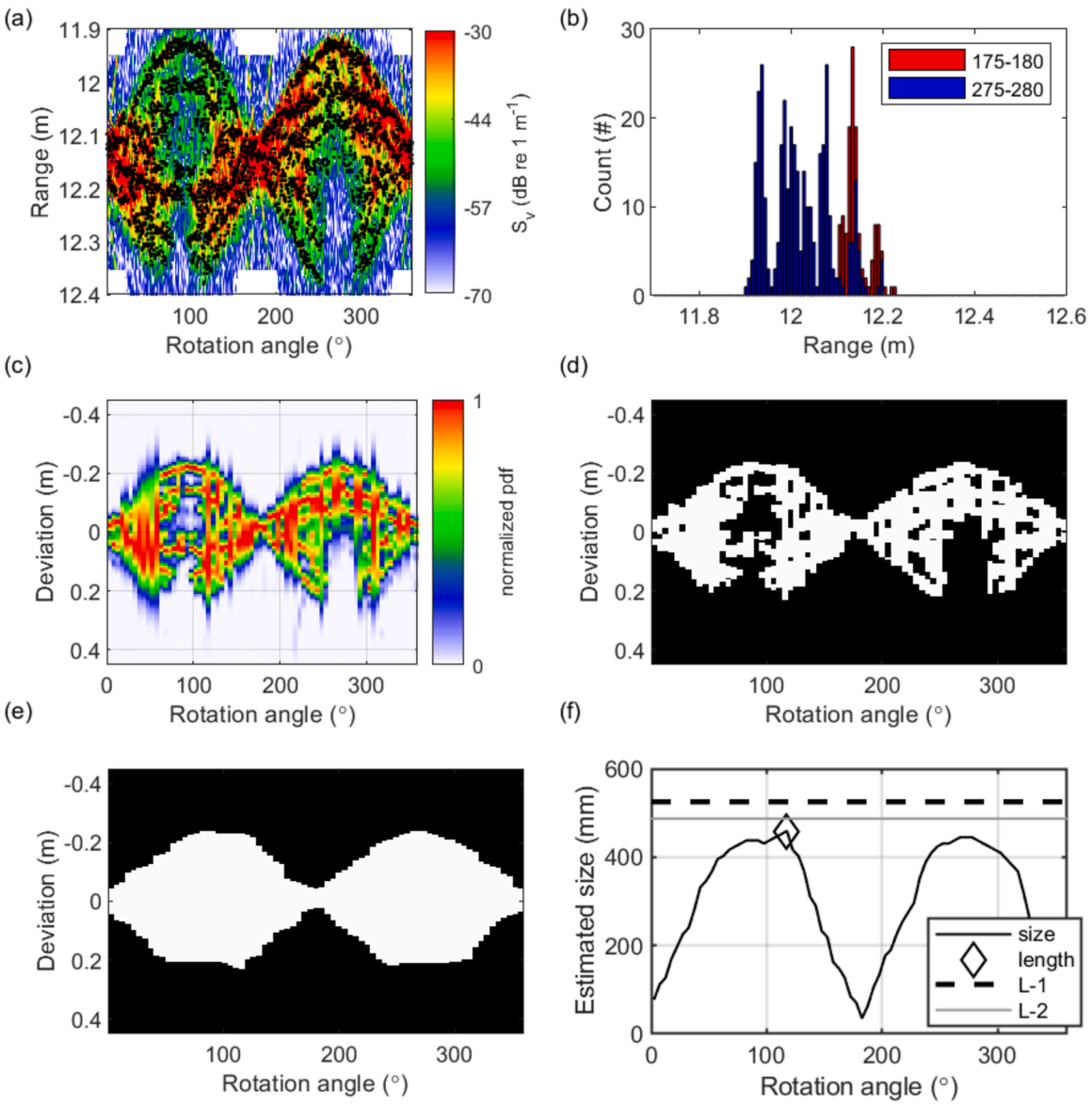

Fig. 6. Example of the statistical processing workflow (160–260 kHz, slow taper, saithe S24) leading to the acoustic fish body length estimate. (a) S_v versus rotation angle with the numerous peak detections (black dots). (b) histograms containing the range-from-transducer for peak detections in two rotation angle bins (175°−180°, red bars and 275°−280°, blue bars). (c) normalised probability density function versus rotation angle. (d) binary image constructed from (c) with a 0.5 threshold. (e) morphological closing on the binary image (d) using a disk element of 10-pixel radius. (f) fish size estimates versus rotation angle. In (f) legend, "size" refers to the estimated fish size as fish body is rotated in the azimuth direction, "length" marked as diamond sign indicates the maximum fish body size observed (458.9 mm here).

mackerel size, however, were much more variable and the adverse effect of a lower SNR (15–17 dB) were evident (Fig. 11). The measured signal to noise ratio for 160–260 kHz data was 15.9 (± 0.5), 18.1 (± 0.9), and 18.6 (± 0.2) dB for mackerel, saithe, and pollack measurements, respectively.

The correlation of the acoustically inferred fish size with the fish standard length (L-2) was strong (Fig. 7 and Table 4) and is the result of an overall strong correlation with effective fish size at oblique angles (Fig. 12a). In contrast, this correlation is poor when fish were observed at broadside aspect with non-significant linear relationships at fish body posture angles close to 0° or 180° (Fig. 12a). The goodness of fit values for 160–260 kHz slow taper pulses were higher across the entire range of target rotation angles compared to the fast taper pulses. The distribution of residuals from each linear regression (Fig. 12b and c) is similar across the rotation angle bins with a smaller deviation in mean values for the slow-tapered signal (Fig. 12c). The r_{est} estimates at various rotation angle bins (Fig. 12d and e) had a ratio close to 1 at oblique fish body angles and a reduced spread compared to fish observations close to broadside angles.

4. Discussion

The ability to detect backscatter peaks associated with fish body boundaries (and by extension, the ability to size the fish) varied with: (1) pulse bandwidth and (2) pulse taper, (3) the signal-to-noise ratio, (4) fish species, (5) fish size, and (6) body orientation with respect to the acoustic wave (Figs. 7, 8, 10, 11, 12). The best remote acoustic sizing results were obtained using 160–260 kHz pulses with slow taper (Fig. 7). Fish body length was generally underestimated (Fig. 8).

The slow tapered pulses at 160–260 kHz were the most effective to size the fish. Whilst useable, results for fast tapered pulses at 160–260 kHz suffered from a higher noise floor coming from more

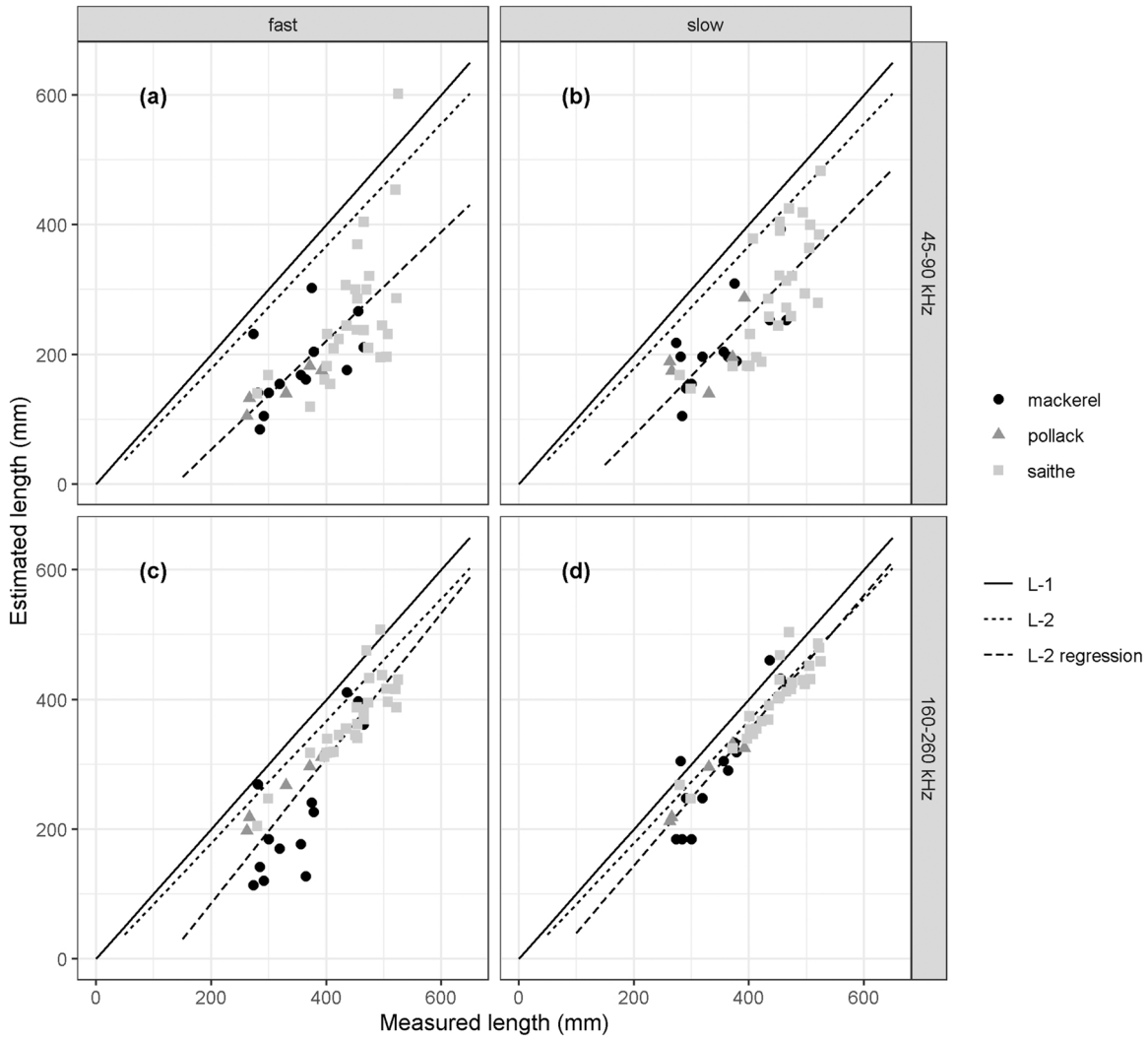

Fig. 7. The acoustic data-derived fish length estimates are given for the four used broadband pulse bandwidth and taper combinations: (a) 45–90 kHz pulses with fast taper, (b) 45–90 kHz pulses with slow taper, (c) 160–260 kHz pulses with fast taper, and (d) is for 160–260 kHz pulses with slow taper. The 1:1 line for the estimated fish length vs. total fish length (L-1) and standard fish length (L-2) are drawn (solid and dotted lines, respectively). The linear regression is examplified as the dashed line in each graph.

pronounced temporal side lobes after matched filtering (Kubilius et al., 2020). Fishes were able to be acoustically sized with the 45–90 kHz bandwidth pulses, but measures were less accurate (Fig. 8a, b) and with higher spread (Fig. 7a, b) when compared to measures obtained with 160–260 kHz pulses (Fig. 7c, d and Fig. 8c, d). This is the result of the lower range resolution of the 45–90 kHz pulses and the expectedly lower signal-to-noise ratio for the soft tissue and small bone echoes that form the outer boundaries of the rotating fish echo (i.e., outer target boundaries were less pronounced, especially at oblique fish angles with respect to the incoming acoustic wave, Fig. 4).

More accurate and less variable fish size estimates were obtained with slow tapered acoustic pulses (Figs. 7, 8) despite their lower range resolution. Broadband pulse compression provides a markedly improved range resolution but suffers from the presence of temporal sidelobes that can be confounding when identifying closely spaced echoes (Kubilius et al., 2020) such as from internal fish boundaries. Therefore, the good performance of the pulse shape that is weighted to suppress these sidelobes (Cook and Bernfeld, 1967) was expected.

Fish body length was underestimated to a similar degree between the three species measured (Fig. 8d). There was no clear length-dependent trend or bias between the true fish length (L-2) and the acoustically derived length for the fish sizes and species measured (Fig. 7) if the SNR was sufficient. Some tendency to undersize smaller fish at various grazing angles was found when comparing acoustically derived fish lengths to x-ray image-derived fish size data (Fig. 11). The acoustic sizing method employed here did not have a significant bias toward the smallest fish lengths. For example, the acoustically derived fish length of the smallest specimen in this study (Pollack, 239 mm) was underestimated by 11.7%. This suggests that the acoustic sizing method presented is applicable to the range of fish sizes considered (239–491 mm) and possibly beyond the lower limit (<239 mm). Saithe and pollack acoustically derived fish size estimates were more successfully obtained when the fish tail was closer to the acoustic transducer than when the head was closer (Fig. 9). The cause of this was not investigated.

The fish size underestimation was expected due to comparatively weak backscattering from the outer parts of the fish body (various soft tissue) and the severely reduced backscattering at head-on/tail-on target angles. The range from the transducer to the tip of the first and last pronounced S_v peaks (e.g., Fig. 5b) are not necessarily echoes from the outermost boundaries of the fish body. This is because the tail and snout generated relatively weak acoustic backscatter. Due to this, the standard fish length (L-2, measured from the tip of fish snout to the posterior end of the last vertebra or the mid-lateral portion of the hypural plate, Fig. 2) was used for comparisons with the acoustic measures as it was more

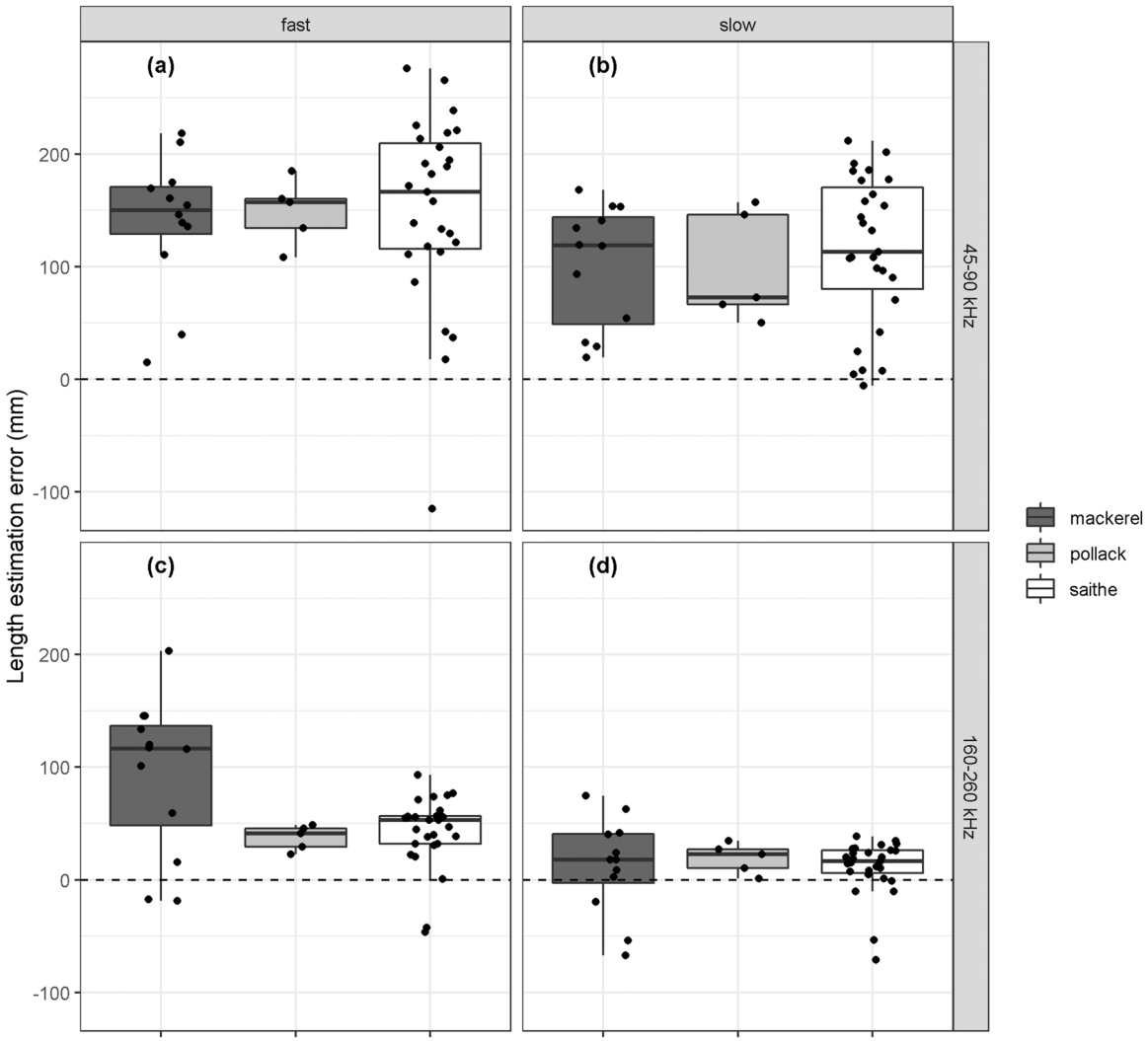

Fig. 8. The fish body length estimation error (relative to L-2 in mm) for the four used broadband pulse bandwidth and taper combinations. The box plot shows the median, first and third quartiles, and box plot whiskers show 5% and 95% confidence intervals. (a) and (b) show results for 45–90 kHz pulses with fast and slow taper, respectively. (c) and (d) show data for 160–260 kHz pulses with fast and slow taper, respectively.

representative of the acoustically visible fish body parts.

The acoustic sizing method performed worse for mackerel than other fishes (Figs. 7, 8, 11). It is unclear if the lower sizing success for mackerel (Fig. 8c, d) is species specific. The mackerel data were not obtained in the same time period as the saithe and pollack, had a lower SNR ratio (Fig. 11) and were collected under more adverse weather conditions (resulting in noticeable relative movements between the target and transducers). The r_{est} distributions for saithe and pollack were similar (Fig. 11) and for the dynamic ranges observed here, the SNR and length class variables did not affect the performance of the acoustic sizing.

The fish sizing method was most successful at oblique fish angles (Figs. 9, 12). The reason for this is three-fold. Firstly, while the total fish echo is strongest when measured at the broadside (Fig. 4), the within-fish boundary transition backscatter peaks are close together and hence hard to distinguish (Fig. 5a). Secondly, the echoes from the vertical nylon suspension lines (Figs. 1, 4) partly overlapped and possibly interfered with the fish echo at broadside angles. Thirdly, the pulse compression temporal side lobes associated with swimbladder backscatter were largest at broadside angles and interfered with the detection of the weaker backscatter peaks from other fish parts, such as the seawater/flesh boundary. Similar results were reported when sizing artificial, prolate-spheroid shaped targets (Kubilius et al., 2020). The acoustic sizing measures in that work were mainly limited by the nominal range resolution of the broadband pulses, SNR of the object-seawater boundary detection, and adverse effects of pulse compression sidelobes adjacent to echoes from the air-filled cavity. In contrast to the work presented here, thickness of the artificial fishes was reliably measured via the amplitude peak detection method (with 160–260 kHz, slow-tapered pulses). The simplicity of the artificial targets meant that the echo from the prolate spheroids contained only well-defined backscatter peaks that corresponded to two or four boundary transitions (seawater/object and object/gas cavity). In contrast, fish contain many internal boundaries (e.g., Figs. 4, 6a) that generate overlapping echo peaks, especially at broadside angles.

The remote fish sizing method described here worked best at oblique fish body angles – these are readily obtained with laterally projected acoustic beams. An envisioned application of the method would be pre-capture sizing of fish during, for example, purse seining operations. Here a fish school is commonly inspected with an omnidirectional sonar while the vessel circles the fish school at a distance of a few hundred meters. A narrow, laterally projected acoustic beam pointed towards the school would then provide individual fish detections from the outskirts of the school at a variety of fish angles. The incidence angle of these targets could be estimated from target tracking over several pings and the sizing methods detailed in this paper applied. Sizing of these targets without knowledge of incidence angle would produce a range of apparent size

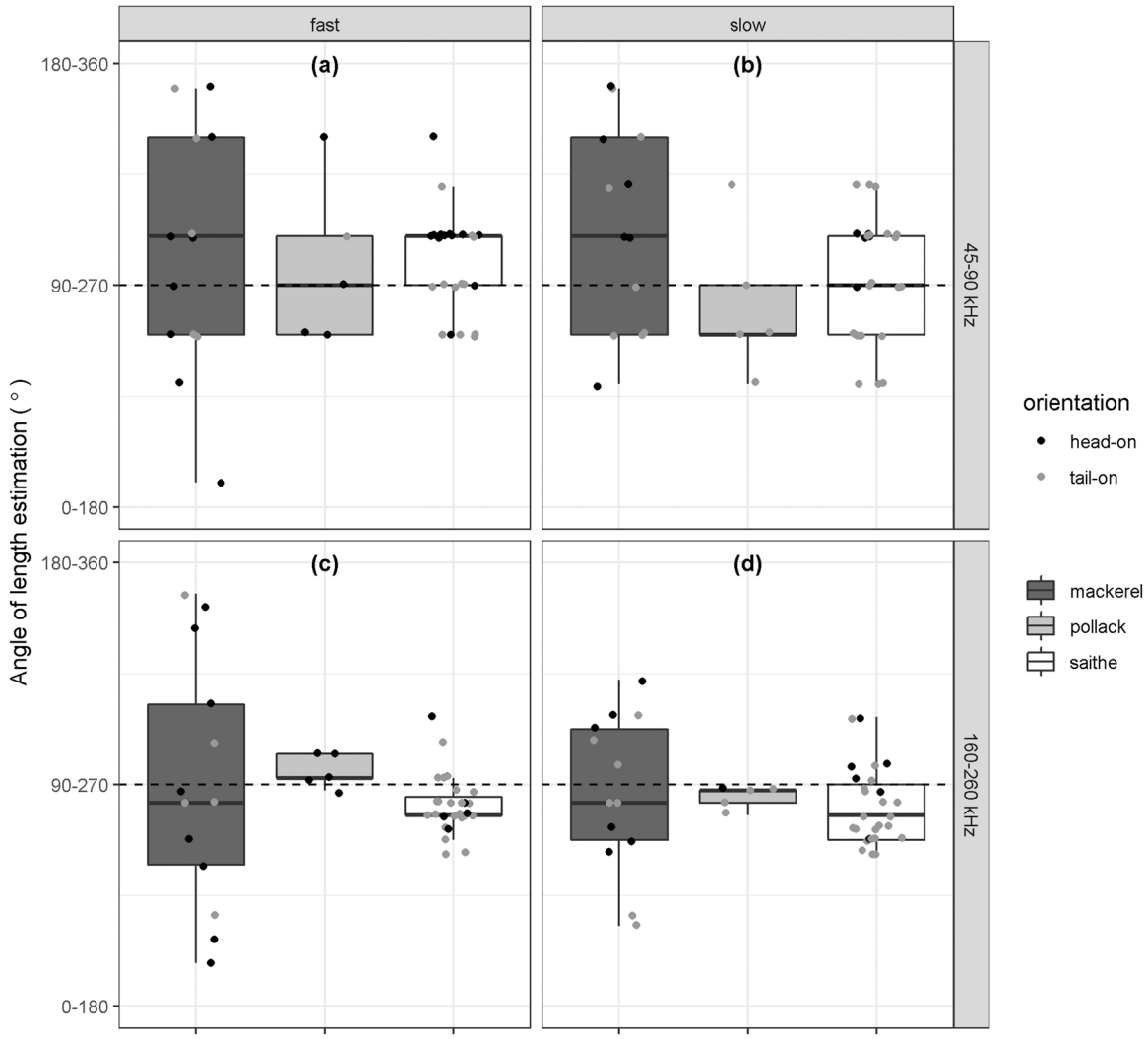

Fig. 9. The fish body rotation angle at which acoustic-derived size estimate was obtained. (a) 45–90 kHz pulses with fast taper, (b) 45–90 kHz pulses with slow taper, (c) 160–260 kHz pulses with fast taper, and (d) is for 160–260 kHz pulses with slow taper. The dashed black line is the 90° or 270° angle, the value at which length estimation is most likely (head to tail or tail to head aspect).

Table 4
Linear regression results for fish total length (L-1) and standard length (L-2) against acoustically derived maximum fish body length at head-on/tail-on aspect as measured at two frequency bands and two pulse tapers. R^2 – goodness of fit. Intercept and residual error are in mm.

	Frequency [kHz]	45–90		160–260	
	Taper	Fast	Slow	Fast	Slow
L-1	Slope	0.84	0.93	1.12	0.99
	Intercept	-117.61	-119.16	-136.56	-39.08
	R^2	0.46	0.61	0.82	0.87
	Residual error	73.76	60.10	41.96	30.77
	p-value	3.4×10^{-7}*	2.6×10^{-10}*	1.2×10^{-17}*	1.5×10^{-20}*
L-2	Slope	0.89	0.98	1.04	1.18
	Intercept	-106.62	-105.13	-25.61	-123.11
	R^2	0.46	0.60	0.86	0.82
	Residual error	73.89	60.76	31.53	41.88
	p-value	3.7×10^{-7}*	4.2×10^{-10}*	4.3×10^{-20}*	1.1×10^{-17}*

* p-value < 0.05 indicates a significant trend.

estimates, the largest of these being close to (but under) the standard fish body length (as demonstrated in this study). The profile of size estimates at various incidence angles could also potentially be used to interpolate more accurate fish size measures. Similar considerations could be employed for laterally projected acoustic beams from other platforms, such as lowered probes, moorings, and autonomous vehicles. Limitations of this method application include reduced signal to noise ratio for measurement at range, ability to resolve individuals, fish movement impact (if any) on sizing aptitude, and target discrimination that is now assumed to be known a priori. The frequency bandwidth and half-power beamwidth of the acoustic beam may need be adapted to these specific observational situations. As per the purse seine fishing

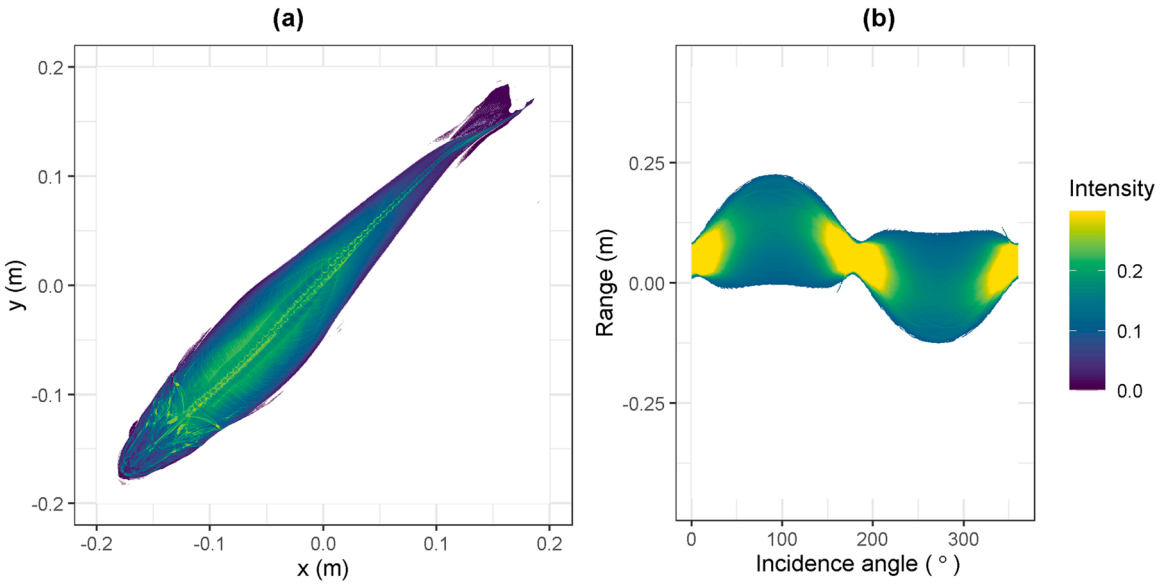

Fig. 10. An example of the simulated acoustic data. (a) a cropped dorsal aspect x-ray image of saithe (S12) and (b) simulated backscatter as a function of range and rotation angle with a colour range that emphasises internal fish structure. Blue colours represent low density and low backscatter, while yellow colours represent high density and backscatter.

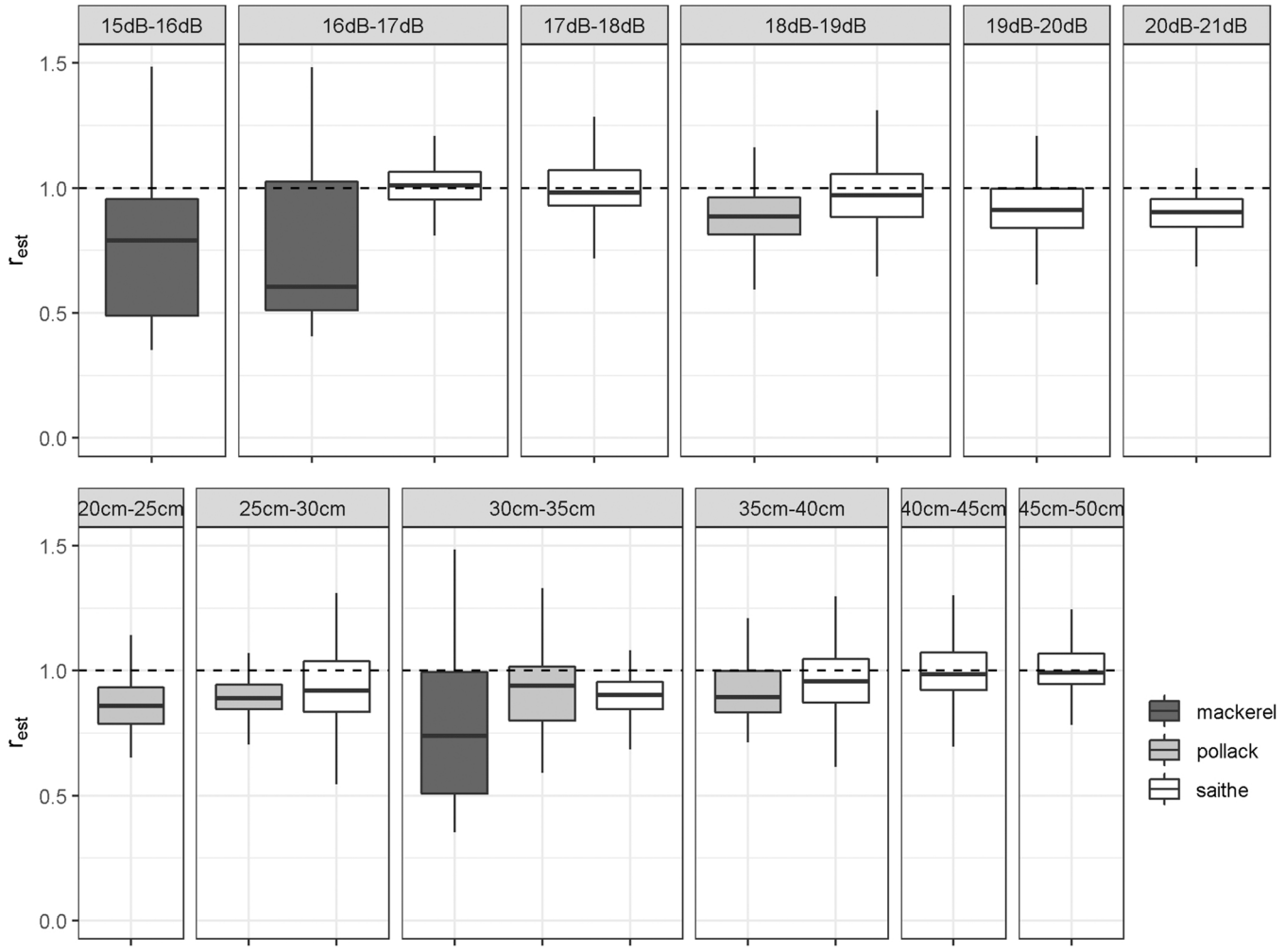

Fig. 11. A boxplot comparison of the fish size estimates obtained from the acoustic (160–260 kHz, slow taper) and x-ray image data. The r_{est} estimates are pooled across the whole 360° azimuth rotation of the fish body. Upper panel: r_{est} estimated for different SNR bins (SNR is marked in the upper part of the plot). Lower panel: r_{est} calculated for a range of fish body length (L-2) bins.

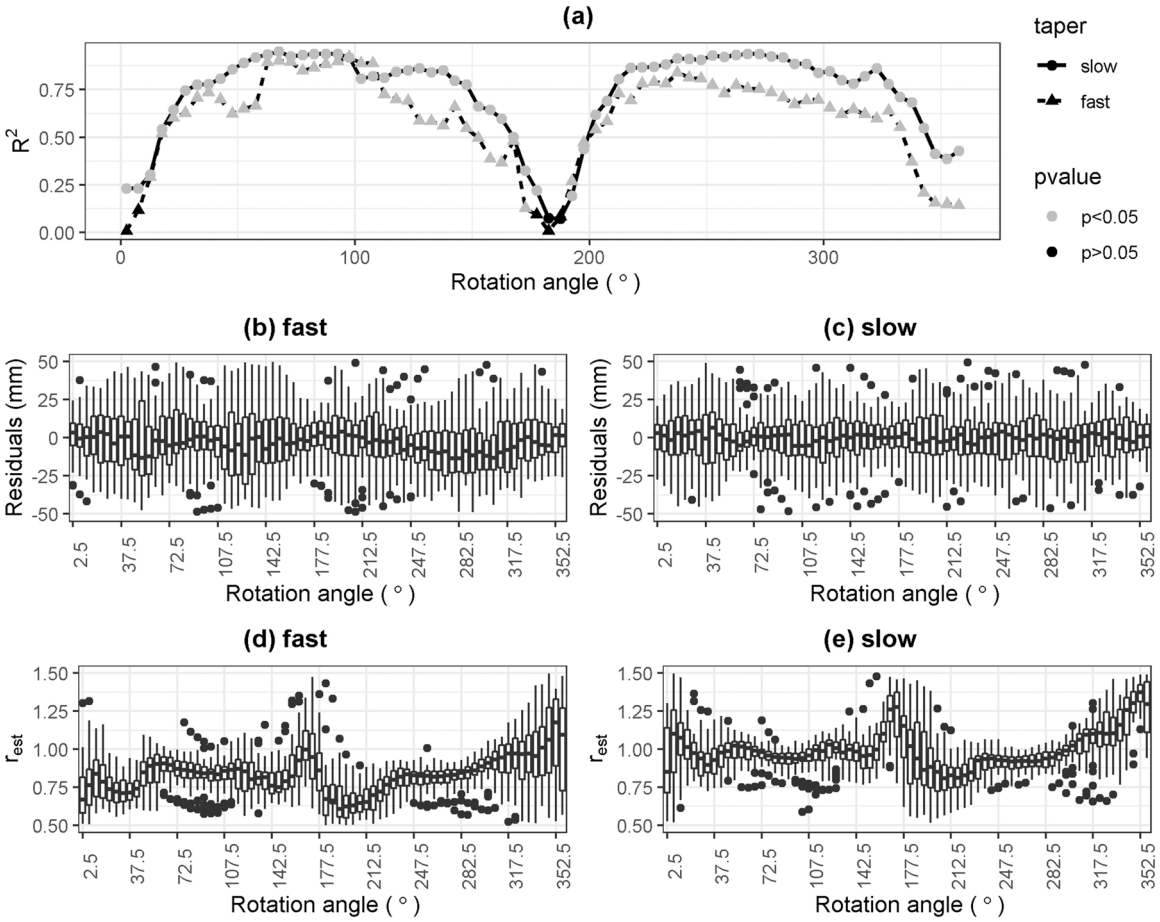

Fig. 12. The comparison of the acoustically derived (160–260 kHz) and the x-ray pseudo-acoustic data-derived fish size estimation at varied target insonification angle. The data is pooled for saithe and pollack. (a): goodness of fit (R^2) of the linear regression in different rotation angle bins for fast taper (dashed black line with triangle markers) and slow taper (solid black line with circle markers). The significance level of the linear relationship as evaluated using p-values is displayed as grey-filled markers (significant, $p < 0.05$) and black-filled markers (not significant, $p > 0.05$). (b) and (c): boxplot of the residuals from the linear regression in each rotation angle bin for fast taper (b) and slow taper (c) data. (d) and (e): boxplot of the ratio between acoustic and x-ray profiles (r_{est}) in different rotation angle bins for fast taper (d) and slow taper (e) data.

example, the 160–260 kHz pulses and 7° wide acoustic beam used in the presented work may not have a sufficient detection range at sea and likely has a too wide acoustic beam for single target separation at a few hundred meters range. In that situation a lower acoustic frequency and narrower acoustic beam would likely be required. If the acoustic beam is oriented vertically downward it is the fish height that is measured. With reduced ability to view the fish at oblique angle, the ability to size fish is reduced for the small to medium size fishes used in this study (thickness of up to 71 mm, Table 1). However, it is expected that height measurements would be successful on larger fish, such as tuna, although broadband pulses may not be necessary as the range resolution of short narrowband pulses could be sufficient and would not have the interference caused by pulse compression temporal sidelobes. While we envision and suggest in situ applications, our experiments were conducted at close range with a favourable signal to noise ratio on immobile fish of known species; the applicability of our method to active fish at far greater ranges (50–200 m) is yet to be determined.

5. Conclusions

This paper presents a method that is suited for direct and remote fish body length measurement but performed less well for measurements of the fish body thickness. More accurate estimates of the fish body width (or height) could be obtained by alternative methods not covered in the present study: (1) measurement of the amplitude peak width (Fig. 5a) that is seen at the broadside observations, and (2) interpretation of dips (commonly referred to as 'nulls') in the broadband frequency response of resolved individual targets.

It has been shown that pulse compressed broadband signals can be used to remotely and directly size fishes with and without swimbladders. The multitude of echo amplitude peaks were resolved within the total scattering from a fish that were associated with fish body boundary transitions (such as bones, swimbladder, and various types of soft tissue). A processing algorithm was presented to autonomously extract fish size estimates. It was most successful for fishes observed at oblique fish angles that are commonly observed with laterally oriented acoustic beams. This work will facilitate in situ and catch-free sizing of free-swimming fishes.

CRediT authorship contribution statement

Rokas Kubilius: Conceptualization, Methodology, Software, Investigation, Writing - original draft, Visualization. **Benoît Bergès:** Methodology, Software, Investigation, Formal analysis, Writing – review & editing, Visualization. **Gavin J. Macaulay:** Conceptualization, Methodology, Investigation, Writing – review & editing, Funding acquisition.

Declaration of Competing Interest

The authors declare that they have no known competing financial

interests or personal relationships that could have appeared to influence the work reported in this paper.

Data availability

Data will be made available on request.

Acknowledgements

This experimental work was funded by the Research Council of Norway under the AcoSize project (no. 255589/E40). CRIMAC project (no. 309512) is also acknowledged for support. We thank Austevoll Research Station (Norway) personnel for their assistance. Atle Totland (IMR, Norway) is thanked for his skilful adaptation and design of the fish rotation motor and its control system.

References

Cook, C.E., Bernfeld, M., 1967. Radar Signals: An Introduction to Theory and Application. Academic Press, p. 550. https://doi.org/10.1016/B978-0-12-186750-8.X5001-7.

Davenport, D., Hakling, W.R., 1965. Method of rapid measurement for large samples of fish. J. Fish. Res. Board Can. 22, 1309–1310. https://doi.org/10.1139/f65-113.

De Robertis, A., Lawrence-Slavas, N., Jenkins, R., Wangen, I., Mordy, C.W., Meinig, C., Levine, M., et al., 2019. Long-term measurements of fish backscatter from Saildrone unmanned surface vehicles and comparison with observations from a noise-reduced research vessel. ICES J. Mar. Sci. 76, 2459–2470. https://doi.org/10.1093/icesjms/fsz124.

Demer, D.A., Berger, L., Bernasconi, M., Bethke, E., Boswell, K., Chu, D., Domokos, R., et al., 2015. Calibration of acoustic instruments. ICES Coop. Res. Rep. No 326, 133. https://doi.org/10.25607/OBP-185.

Ehrenberg, J.E., Torkelson, T.C., 2000. FM slide (chirp) signals: a technique for significantly improving the signal-to-noise performance in hydroacoustic assessment systems. Fish. Res. 47, 193–199. https://doi.org/10.1016/S0165-7836(00)00169-7.

Fofonoff, N.P., Millard Jr, R.C., 1983. Algorithms for the computation of fundamental properties of seawater. UNESCO Tech. Pap. Mar. Sci. 44, 53. https://doi.org/10.25607/OBP-1450.

Forland, T.N., Hobæk, H., Korneliussen, R.J., 2014. Scattering properties of Atlantic mackerel over a wide frequency range. ICES J. Mar. Sci. 71, 1904–1912. https://doi.org/10.1093/icesjms/fsu045.

Francois, R.E., Garrison, G.R., 1982. Sound absorption based on ocean measurements. Part II: boric acid contribution and equation for total absorption. J. Acoust. Soc. Am. 72, 1879–1890. https://doi.org/10.1121/1.388673.

Hawkins, A.D., 1977. Fish sizing by means of swimbladder resonance. ICES Rep. 170, 122–129.

Huse, I., Vold, A., 2010. Mortality of mackerel (Scomber scombrus L.) after pursing and slipping from a purse seine. Fish. Res. 106, 54–59. https://doi.org/10.1016/j.fishres.2010.07.001.

Johnsen, E., Pedersen, R., Ona, E., 2009. Size-dependent frequency response of sandeel schools. ICES J. Mar. Sci. 66, 1100–1105. https://doi.org/10.1093/icesjms/fsp091.

Kubilius, R., Macaulay, G.J., Ona, E., 2020. Remote sizing of fish-like targets using broadband acoustics. Fish. Res. 228, 105568 https://doi.org/10.1016/j.fishres.2020.105568.

MacLennan, D.N., Fernandes, P.G., Dalen, J., 2002. A consistent approach to definitions and symbols in fisheries acoustics. ICES J. Mar. Sci. 59, 365–369. https://doi.org/10.1006/jmsc.2001.1158.

McClatchie, S., Alsop, J., Coombs, R.F., 1996. A re-evaluation of relationships between fish size, acoustic frequency, and target strength. ICES J. Mar. Sci. 53, 780–791. https://doi.org/10.1006/jmsc.1996.0099.

Muñoz-Benavent, P., Andreu-García, G., Valiente-González, J.M., Atienza-Vanacloig, V., Puig-Pons, V., Espinosa, V., 2018. Automatic Bluefin Tuna sizing using a stereoscopic vision system. ICES J. Mar. Sci. 75, 390–401. https://doi.org/10.1093/icesjms/fsx151.

Øvredal, J.T., Totland, B., 2002. The scantrol FishMeter for recording fish length, weight and biological data. Fish. Res. 55, 325–328. https://doi.org/10.1016/S0165-7836(01)00274-0.

Poos, J.J., Bogaards, J.A., Quirijns, F.J., Gillis, D.M., Rijnsdorp, A.D., 2010. Individual quotas, fishing effort allocation, and over-quota discarding in mixed fisheries. ICES J. Mar. Sci. 67, 323–333. https://doi.org/10.1093/icesjms/fsp241.

Rosen, S., Holst, J.C., 2013. DeepVision in-trawl imaging: sampling the water column in four dimensions. Fish. Res. 148, 64–73. https://doi.org/10.1016/j.fishres.2013.08.002.

Shortis, M., Harvey, E., Abdo, D., 2009. A review of underwater stereo-image measurement for marine biology and ecology applications. In: Gibson, R.N., Atkinson, R.J.A., Gordon, J.D.M. (Eds.), In Oceanography and Marine Biology: An Annual Review, 360. CRC Press, Boca Raton, pp. 257–292. https://doi.org/10.1201/9781420094220.

Simmonds, E.J., MacLennan, D.N., 2005. Fisheries Acoustics: Theory and Practice. Blackwell Science, Oxford, p. 437. https://doi.org/10.1002/9780470995303.

Stanton, T.K., Reeder, D.B., Jech, J.M., 2003. Inferring fish orientation from broadband-acoustic echoes. ICES J. Mar. Sci. 60, 524–531. https://doi.org/10.1016/S1054-3139(03)00032-8.

Stanton, T.K., Chu, D., Jech, J.M., Irish, J.D., 2010. New broadband methods for resonance classification and high-resolution imagery of fish with swimbladders using a modified commercial broadband echosounder. ICES J. Mar. Sci. 67, 365–378. https://doi.org/10.1093/icesjms/fsp262.

Strachan, N.J.C., 1994. Sea trials of a computer vision based fish species sorting and size grading machine. Mechatronics 4, 773–783. https://doi.org/10.1016/0957-4158(94)90052-3.

Tenningen, M., Vold, A., Olsen, R.E., 2012. The response of herring to high crowding densities in purse-seines: survival and stress reaction. ICES J. Mar. Sci. 69, 1523–1531. https://doi.org/10.1093/icesjms/fss114.

Wollaston, H.J.B., 1928. New Apparatus for measuring Fish. ICES J. Mar. Sci. 3, 380–381. https://doi.org/10.1093/icesjms/3.3.380.